

# New signals in the frequency dependent angular power spectrum?

Olivier Doré

JPL/Caltech

# Outline

---

- CMB observations and the production of chemical elements at the end of the dark ages (*resonant scattering of CMB on metals and ions*)

Basu, Hernandez-Monteagudo, Sunyaev 2004

- Carbon monoxide as CMB foreground

Rhigi, Hernandez-Monteagudo, Sunyaev 2008

# Effect of scattering on CMB temperature

- **Damping:** blending of photons from different line of sight

$$\begin{aligned} \bar{T} + \Delta T &\rightarrow (\bar{T} + \Delta T) - (\bar{T} + \Delta T)(1 - e^{-\tau}) + \bar{T}(1 - e^{-\tau}) \\ &\rightarrow \bar{T} + \Delta T e^{-\tau} \end{aligned}$$

$$C_\ell = C_\ell e^{-2\tau}$$

(Ignore scale dependence here)

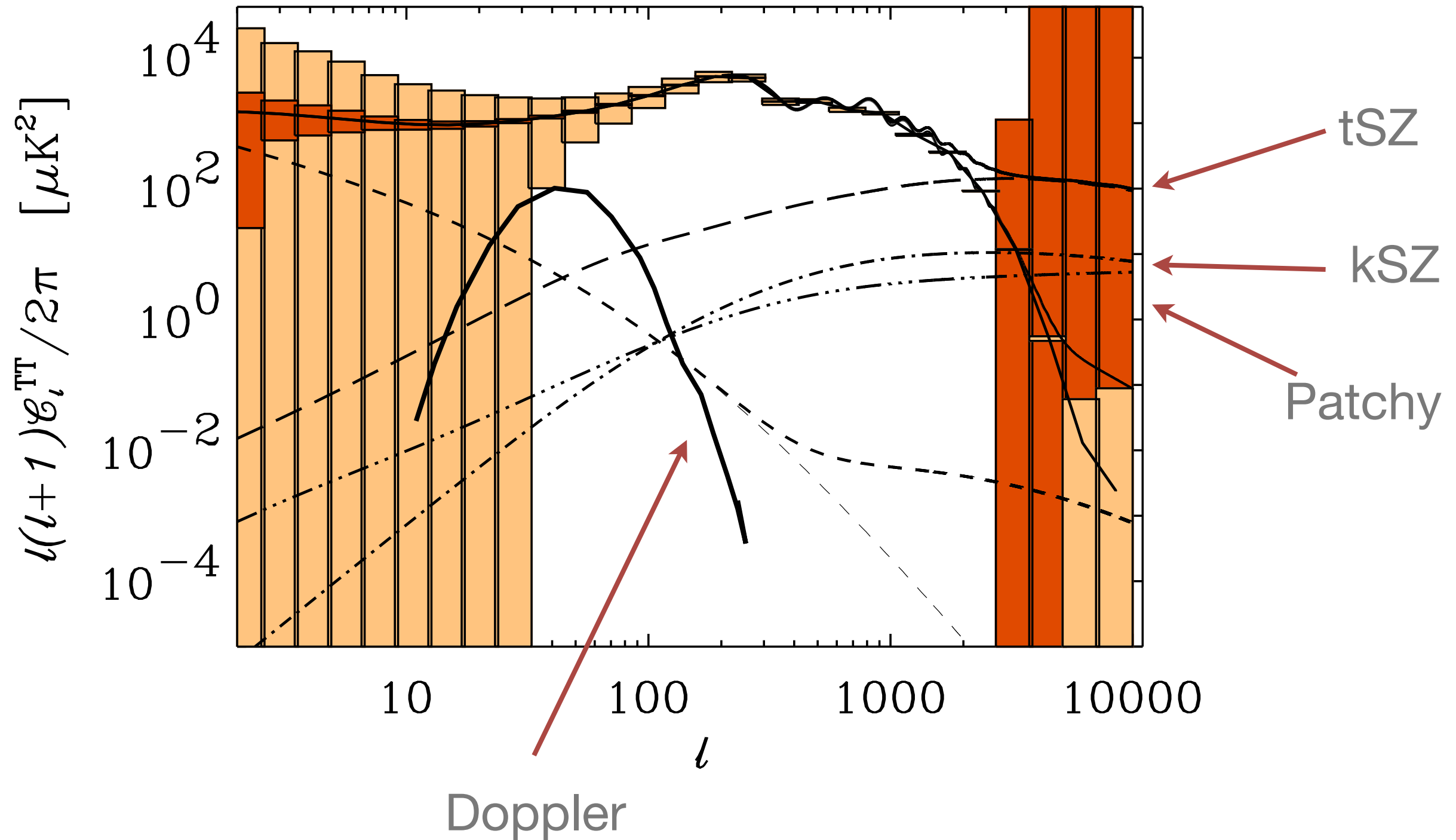
30% suppression for  $l$  greater than 40 (thus hard to measure absolute normalization of the initial conditions)

$$\frac{\Delta T}{T}(\hat{n}) = \sigma_T \int_{\eta_{ion}}^{\eta_0} d\eta x_e(\hat{x}) n_p(\hat{x}) \hat{n} \cdot v_e(\hat{x})$$

- **Doppler effects:** cancellation along the line of sight due to the variation in  $n$ 
  - Except large scales:  $l \sim 100$
  - Reduced if modulation in  $n_p$ : Ostriker-Vishniac effect (kinetic Sunyaev-Zeldovich)
  - Reduced if modulations in  $x_e$ : Patchy reionization

see Knox & Haiman 99 for a review

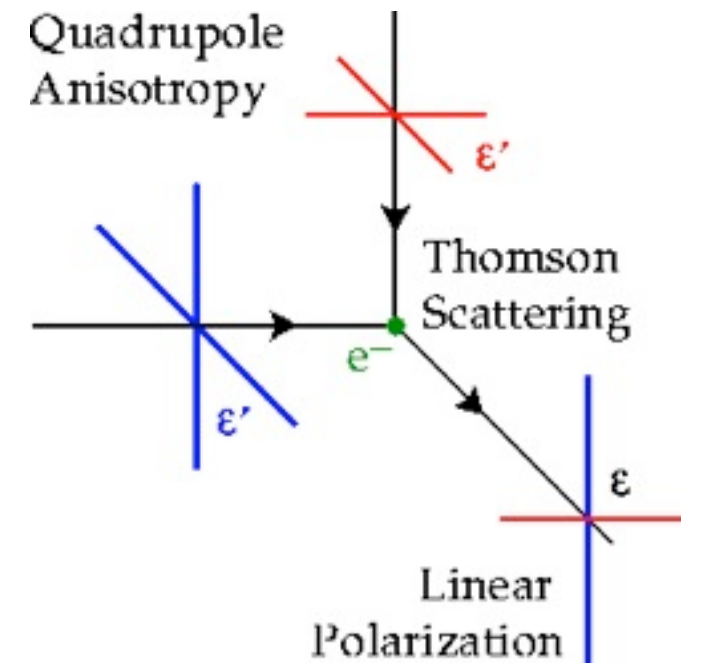
# Effect of reionization on CMB temperature



OD, Hennawi, Spergel 04

# CMB polarization primer

- Linear polarization of the CMB is:
  - Produced by Thomson scattering of a quadrupolar radiation pattern on free electrons: probes both recombination and reionization
  - Partially correlated with temperature (velocity pert. correlates with density pert.)
- Expected signal is an excess power in polarization at the scale of the horizon at the time of reionization ([Zaldarriaga 97](#))



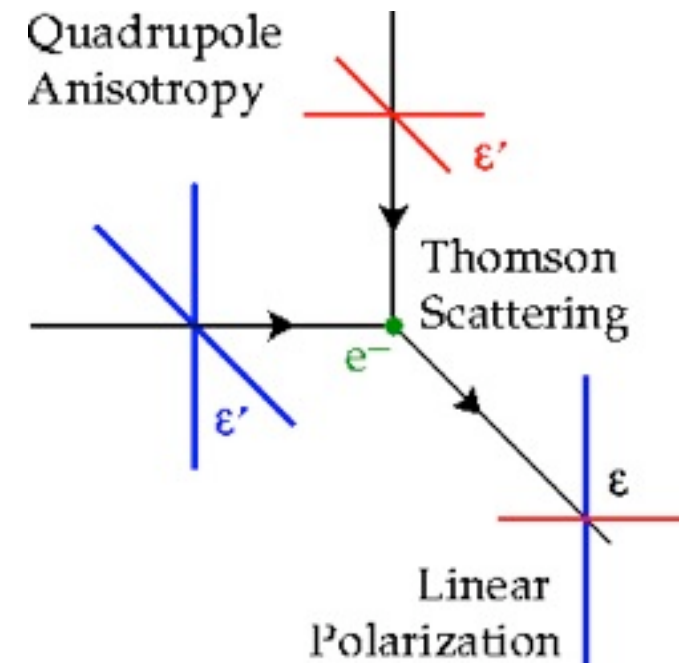
(from W. Hu)

$\propto T$

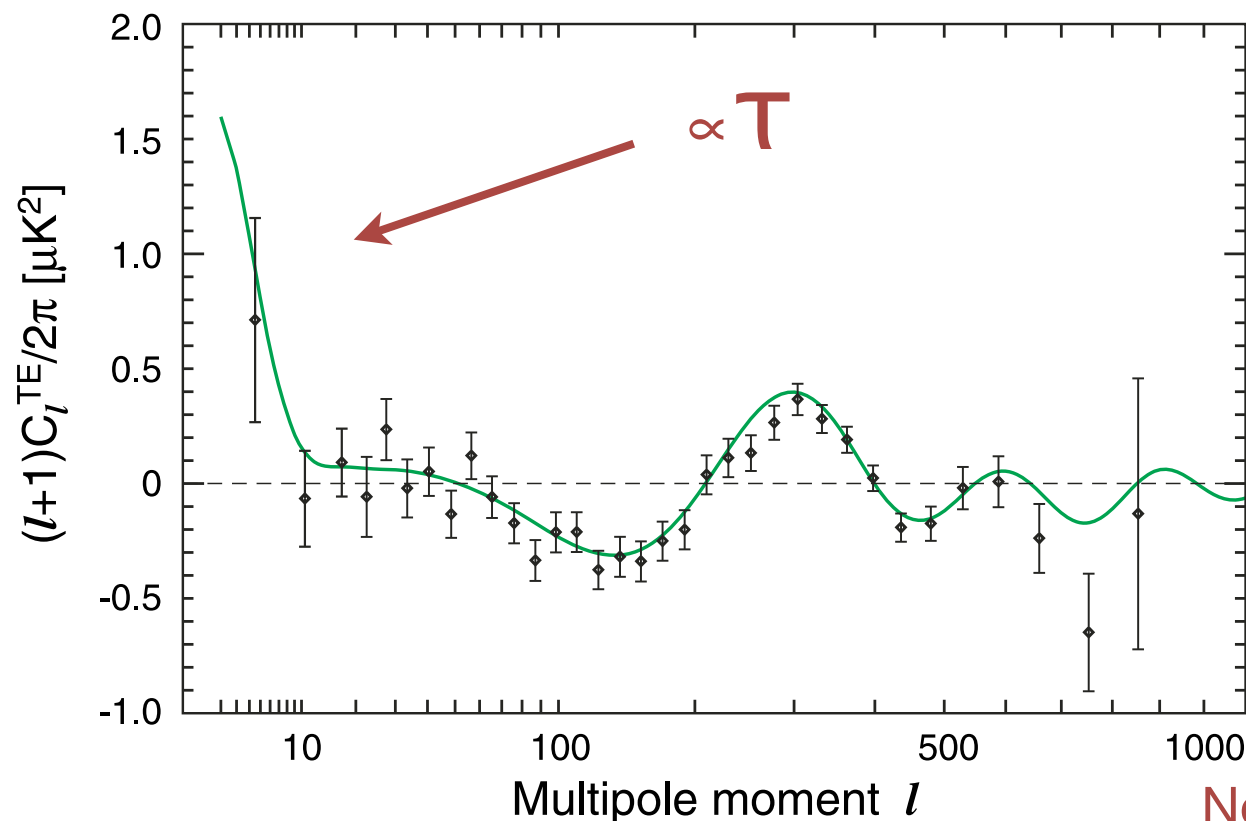
$\propto T^2$

# CMB polarization primer

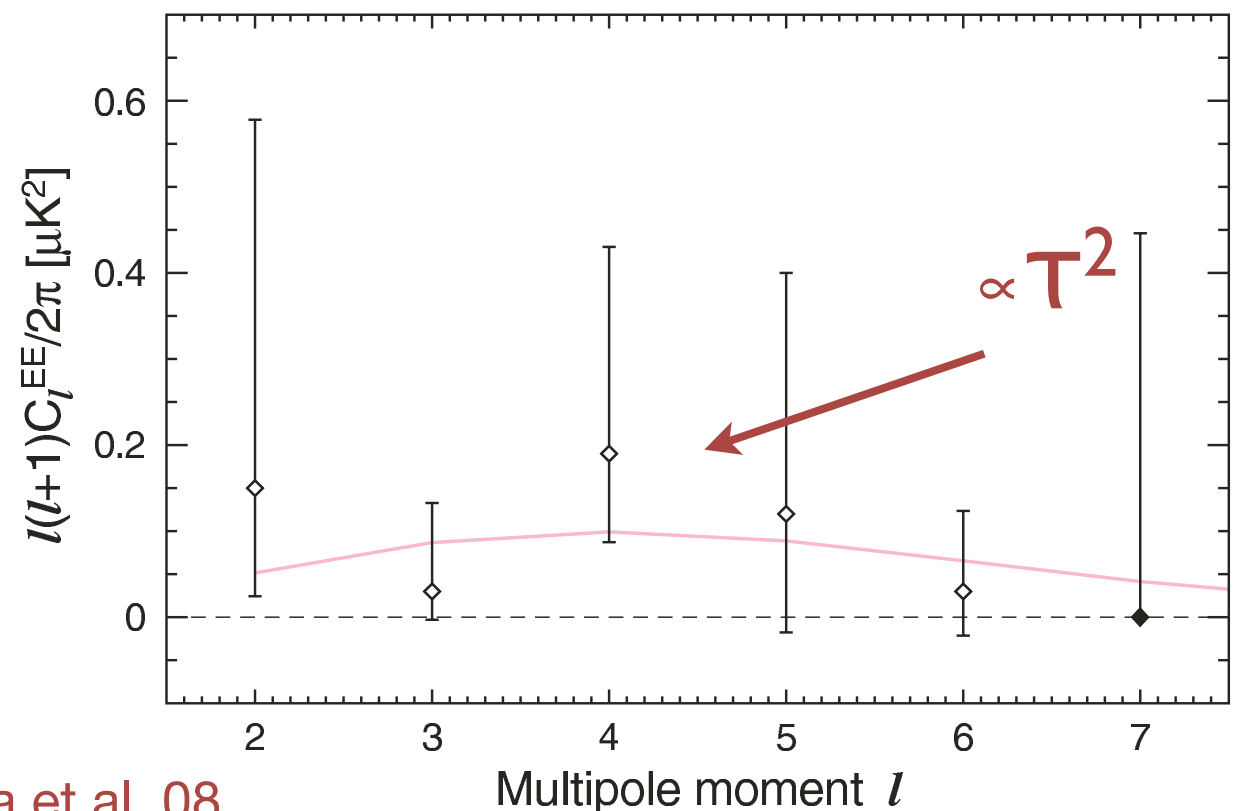
- Linear polarization of the CMB is:
  - Produced by Thomson scattering of a quadrupolar radiation pattern on free electrons: probes both recombination and reionization
  - Partially correlated with temperature (velocity pert. correlates with density pert.)
- Expected signal is an excess power in polarization at the scale of the horizon at the time of reionization (Zaldarriaga 97)



(from W. Hu)



Nolta et al. 08



# Resonant scattering and the CMB

---

- Resonant scattering of atoms and ions, either an atomic or a rotational/vibrational transition
- Origins of heavy elements in the IGM: massive stars, SNe explosions, stellar and galactic winds, etc.
- Scattering phenomenology identical, but optical depth become frequency dependent

$$\tau = \tau_T + \sum_i \tau_{X_i} \qquad \tau_{X_i} = f_i \frac{\pi e^2}{m_e c} \frac{\lambda_i n_{X_i}(z)}{H(z)}$$

$$\delta C_\ell = -2\tau_X C_\ell$$

# Motivations and approximations

---

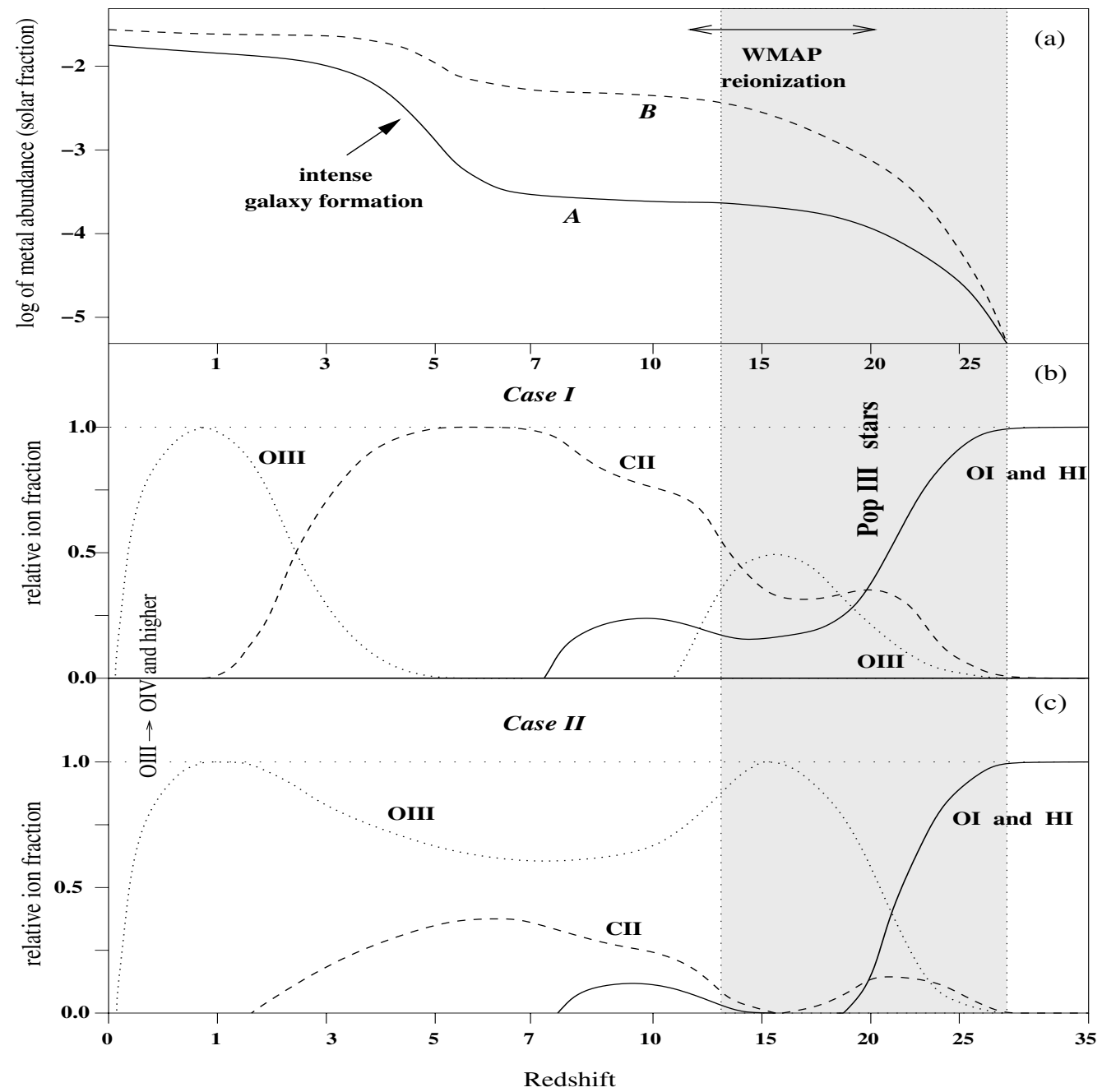
- Scientific goals:
  - Trace the metal enrichment as a function of  $z$
  - Details of reionization
  - Missing baryons
- Homogeneous low density, no perturbations
- Resonant scattering

# Elements studied

Atom/ Ion	Wavelength (in $\mu$ )	Oscillator strength	HFI freq. (GHz)	Scattering redshift	$\mathcal{B}$ factor	Opt. depth for $10^{-2}$ solar abundance	$[X]_{\min}$ for $l = 10$	$\langle [X]_{\min} \rangle$ in $l = 10-20$
<b>C I</b>	609.70	$1.33 \times 10^{-9}$	143	2.4	0.76	$6.4 \times 10^{-6}$	$5.3 \times 10^{-3}$	$2.6 \times 10^{-3}$
			217	1.3	0.92	$3.9 \times 10^{-6}$	$1.4 \times 10^{-2}$	$6.8 \times 10^{-3}$
			353	0.4	0.99	$1.6 \times 10^{-6}$	$2.1 \times 10^{-1}$	$1.2 \times 10^{-1}$
	370.37	$9.08 \times 10^{-10}$	143	4.7	0.15	$1.2 \times 10^{-6}$	$2.8 \times 10^{-2}$	$1.3 \times 10^{-2}$
			217	2.8	0.09	$3.7 \times 10^{-7}$	$1.6 \times 10^{-1}$	$8.1 \times 10^{-2}$
	<b>C II</b>	157.74	$1.71 \times 10^{-9}$	143	12.3	0.79	$1.8 \times 10^{-5}$	$2.7 \times 10^{-2}$
217				7.9	0.94	$1.1 \times 10^{-5}$	$7.7 \times 10^{-3}$	$3.0 \times 10^{-3}$
353				4.4	0.99	$5.6 \times 10^{-6}$	$7.7 \times 10^{-2}$	$3.6 \times 10^{-2}$
<b>N II</b>	205.30	$3.92 \times 10^{-9}$	143	9.2	0.76	$1.1 \times 10^{-5}$	$7.6 \times 10^{-3}$	$2.6 \times 10^{-3}$
			217	5.8	0.92	$6.8 \times 10^{-6}$	$8.6 \times 10^{-3}$	$3.8 \times 10^{-3}$
			353	3.1	0.99	$3.5 \times 10^{-6}$	$1.3 \times 10^{-1}$	$6.8 \times 10^{-2}$
	121.80	$2.74 \times 10^{-9}$	143	16.2	0.16	$2.1 \times 10^{-6}$	$1.3 \times 10^{-1}$	$3.8 \times 10^{-2}$
			217	10.5	0.09	$6.4 \times 10^{-7}$	$3.4 \times 10^{-1}$	$1.1 \times 10^{-1}$
	<b>N III</b>	57.32	$4.72 \times 10^{-9}$	143	35.6	0.79	$2.5 \times 10^{-5}$	$2.3 \times 10^{-3}$
217				23.4	0.94	$1.5 \times 10^{-5}$	$6.1 \times 10^{-3}$	$2.0 \times 10^{-3}$
<b>O I</b>	63.18	$3.20 \times 10^{-9}$	143	32.2	0.88	$1.0 \times 10^{-4}$	$5.3 \times 10^{-4}$	$1.7 \times 10^{-4}$
			217	21.2	0.96	$6.3 \times 10^{-5}$	$2.0 \times 10^{-3}$	$6.4 \times 10^{-4}$
			353	12.5	1.00	$3.1 \times 10^{-5}$	$2.2 \times 10^{-1}$	$4.9 \times 10^{-2}$
<b>O III</b>	88.36	$9.16 \times 10^{-9}$	143	22.8	0.76	$2.2 \times 10^{-4}$	$3.5 \times 10^{-4}$	$1.2 \times 10^{-4}$
			217	14.8	0.92	$1.4 \times 10^{-4}$	$8.4 \times 10^{-3}$	$1.8 \times 10^{-3}$
			353	8.6	0.99	$7.4 \times 10^{-5}$	$1.2 \times 10^{-2}$	$4.4 \times 10^{-3}$
	51.81	$6.55 \times 10^{-9}$	143	39.5	0.17	$4.5 \times 10^{-5}$	$1.4 \times 10^{-3}$	$4.7 \times 10^{-4}$
			217	26.0	0.10	$1.4 \times 10^{-5}$	$6.5 \times 10^{-3}$	$2.2 \times 10^{-3}$
	<b>Si I</b>	129.68	$6.24 \times 10^{-9}$	143	15.2	0.76	$6.4 \times 10^{-6}$	$6.9 \times 10^{-2}$
217				9.8	0.92	$4.2 \times 10^{-6}$	$3.7 \times 10^{-2}$	$1.2 \times 10^{-2}$
68.47		$4.92 \times 10^{-9}$	143	29.7	0.19	$1.8 \times 10^{-6}$	$3.1 \times 10^{-2}$	$1.0 \times 10^{-2}$
<b>Si II</b>	34.81	$7.74 \times 10^{-9}$	217	39.2	0.94	$2.0 \times 10^{-5}$	$4.8 \times 10^{-3}$	$1.6 \times 10^{-3}$
			353	23.4	0.99	$1.0 \times 10^{-5}$	$7.4 \times 10^{-3}$	$2.4 \times 10^{-2}$
<b>S I</b>	25.25	$8.03 \times 10^{-9}$	217	54.4	0.96	$6.0 \times 10^{-6}$	$2.4 \times 10^{-2}$	$7.4 \times 10^{-3}$
<b>Fe I</b>	24.04	$1.69 \times 10^{-8}$	143	86.4	0.83	$3.2 \times 10^{-5}$	$4.9 \times 10^{-3}$	$1.3 \times 10^{-3}$
			217	57.2	0.95	$2.0 \times 10^{-5}$	$7.7 \times 10^{-3}$	$2.3 \times 10^{-3}$
			353	34.4	0.99	$9.7 \times 10^{-6}$	$7.5 \times 10^{-2}$	$2.5 \times 10^{-2}$
	34.71	$2.06 \times 10^{-8}$	143	59.5	0.02	$9.2 \times 10^{-7}$	$1.1 \times 10^{-1}$	$3.4 \times 10^{-2}$
<b>Fe II</b>	25.99	$1.73 \times 10^{-8}$	217	52.9	0.95	$1.9 \times 10^{-5}$	$7.1 \times 10^{-3}$	$2.2 \times 10^{-3}$
			353	31.7	0.99	$1.3 \times 10^{-7}$	$7.4 \times 10^{-2}$	$2.4 \times 10^{-2}$
<b>Fe III</b>	22.93	$3.09 \times 10^{-8}$	353	36.1	0.99	$1.8 \times 10^{-5}$	$4.2 \times 10^{-2}$	$1.4 \times 10^{-2}$

- Fine structure transitions for atoms and ions
- Neutral atoms or singly/doubly ionized heavy elements

# Chemical abundances over time



# Abundances as a function of frequency

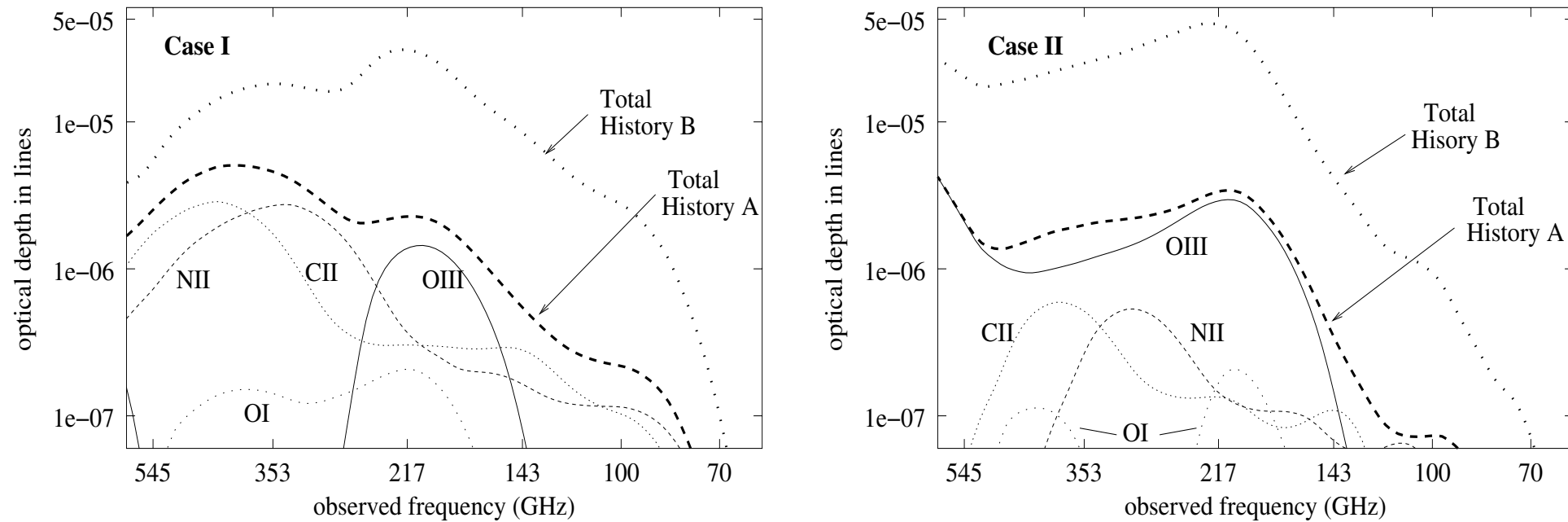


**Fig. 3.** *Top:* a schematic diagram for the abundance history of the universe. **a)** The upper panel shows the global pattern of metal abundances, showing the two major epochs of enrichment of the IGM: first, during the peak of activity of massive Pop III stars around redshift 15–25 (*shaded area*), and second, during the peak of galaxy formation around redshift 3–5 when global rate of star formation reaches maximum. **b)** Middle panel shows the relative fraction of three major atomic and ionic species: OI (or HI), CII and OIII, normalized so that the total abundance of all ions of a given element is close to unity at any redshift. The OI abundance closely follows the neutral hydrogen fraction of the universe because their almost similar ionization potential (see discussion in text). The redshift scale is chosen as  $\log(z + 5)$  to emphasize the redshift region 10–30 of interest to this paper. At very low redshifts ( $z < 0.7$ ) the IGM gets heated to very high temperatures ( $T \sim 10^5 - 10^7$  K) causing even higher ionized species to exist, e.g. OIII  $\rightarrow$  OVI. **c)** Lower panel shows another variation of relative ion fraction, where Pop III stars ionize all the oxygen around redshift 15, so that OIII have higher abundance and correspondingly OI and CII have lower abundance. *Bottom:* frequency dependence of optical depth in atomic and ionic fine-structure lines, in accordance with the abundance history sketched above. Shown here are the contributions from the four most important lines: neutral oxygen  $63 \mu$ , doubly ionized oxygen  $88 \mu$ , singly ionized nitrogen  $205 \mu$  and singly ionized carbon  $158 \mu$ , and their total contribution for each histories. History of NII ion is taken as similar to that of CII ion.

# Contribution to $C_l$

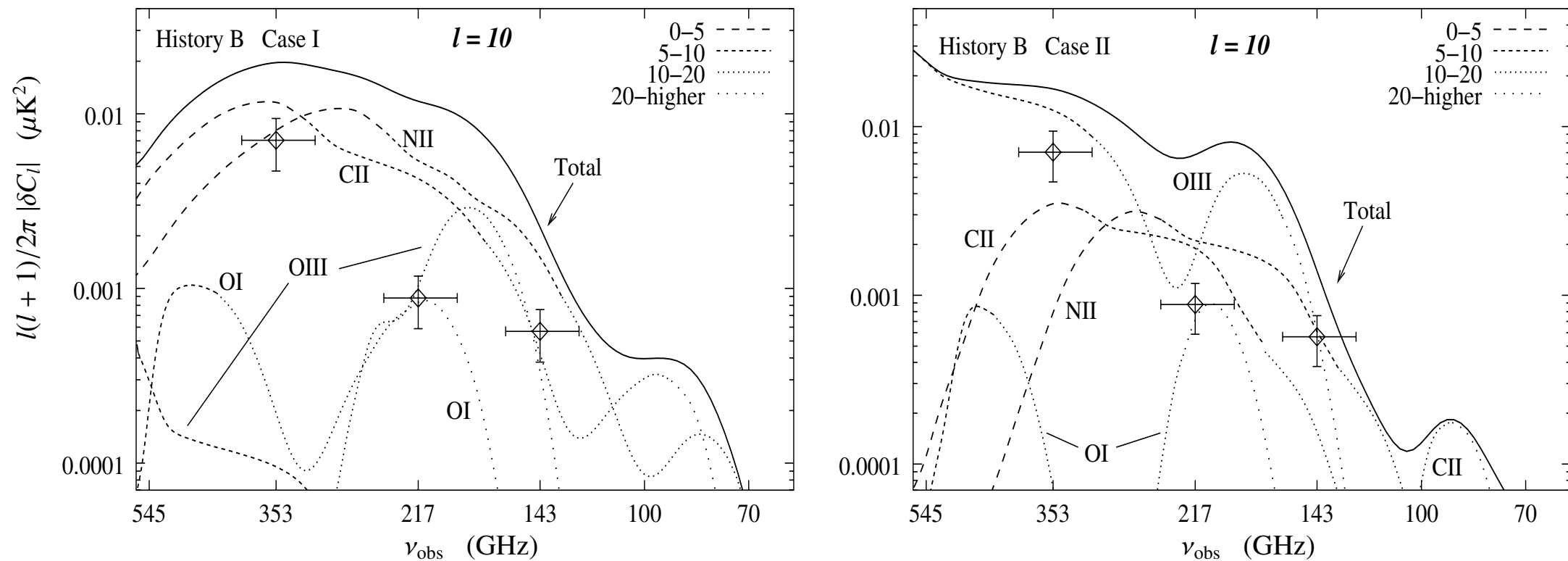


**Fig. 4.** Frequency dependence of temperature anisotropy generated by scattering from fine-structure lines. We take two ionization histories and the high abundance case from Fig. 3, and show the contributions of different lines in different frequency range, for a fixed multipole  $l = 10$ . Four different redshift ranges are marked for each species to emphasize the epochs where the dominant contribution from each lines are coming. The sensitivity limits of Planck HFI channels are marked by the crosses. The HFI limits have been improved by a factor of  $\sqrt{\Delta l}$  by averaging over in the multipole range  $l = 7-16$ . The sensitivity limits are for 3 standard deviation detection, and the  $y$ -errorbars correspond to  $1\sigma$  error in  $3\sigma$  detection (we recall that  $\sigma = 3 \sqrt{\sigma_{C_l(\text{probe})}^2 + \sigma_{C_l(\text{ref})}^2}$ , where the reference channel is fixed at HFI 100 GHz). The  $x$ -errorbars corresponds to the wide bandwidth ( $\sim 25\%$ ) of Planck HFI channels.

# One example

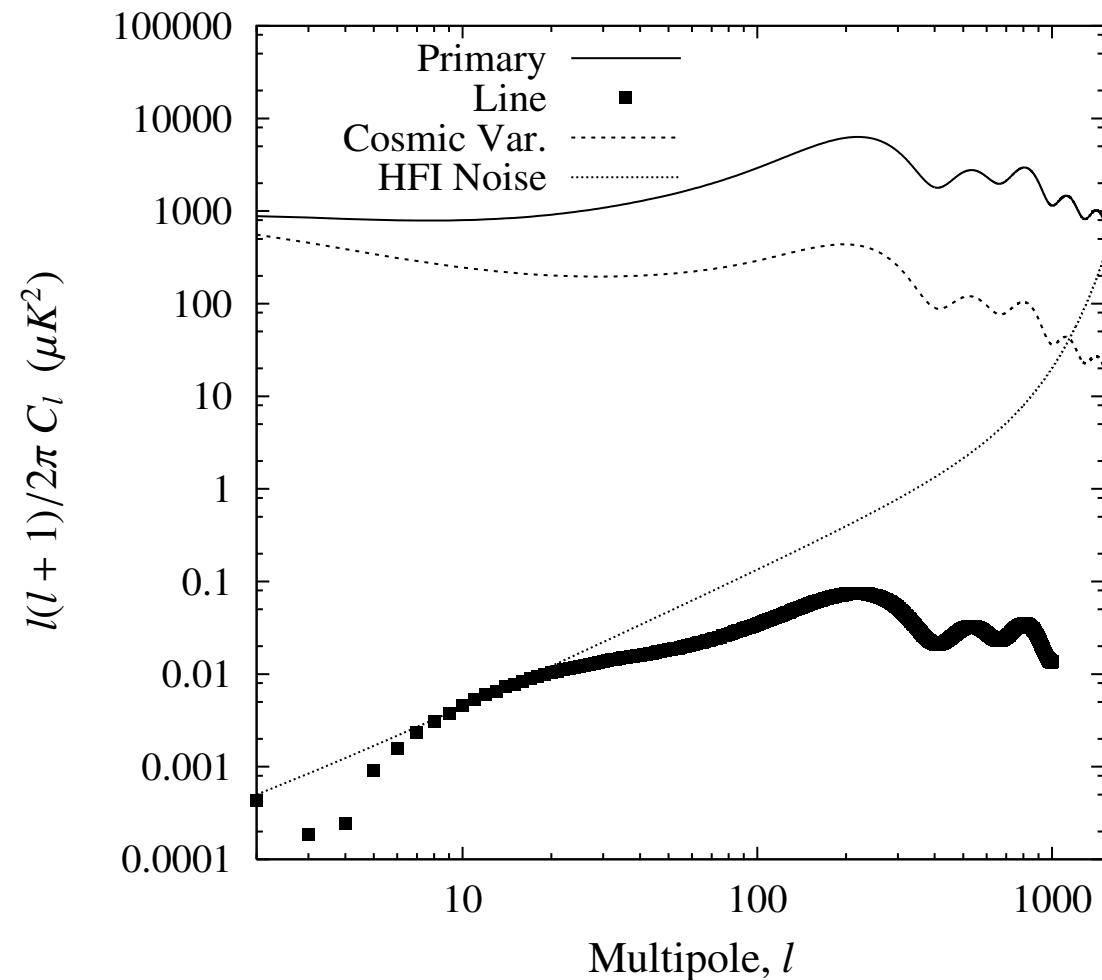


**Fig. 1.** The nature of temperature anisotropy that will be marginally detectable with Planck HFI 143 GHz channel, using  $63 \mu$  OI line. Abundance is taken from the Table 1, as  $5.3 \times 10^{-4}$  solar at redshift 32. Here Primary denotes the measured temperature anisotropy (*upper line*),  $C_l^{\text{pri}} + \delta C_l \approx C_l^{\text{pri}}$ , and Line denotes the the newly generated anisotropy,  $|\delta C_l|$ , arising from line scattering (*bottom, with filled squares*). This  $|\delta C_l|$  is obtained by taking the difference from the 100 GHz channel, and changes sign around  $l = 3$ . The corresponding noise level is denoted by HFI noise. Also shown is the cosmic variance limit (*short-dashed line*) for comparison.

# Planck forecasts

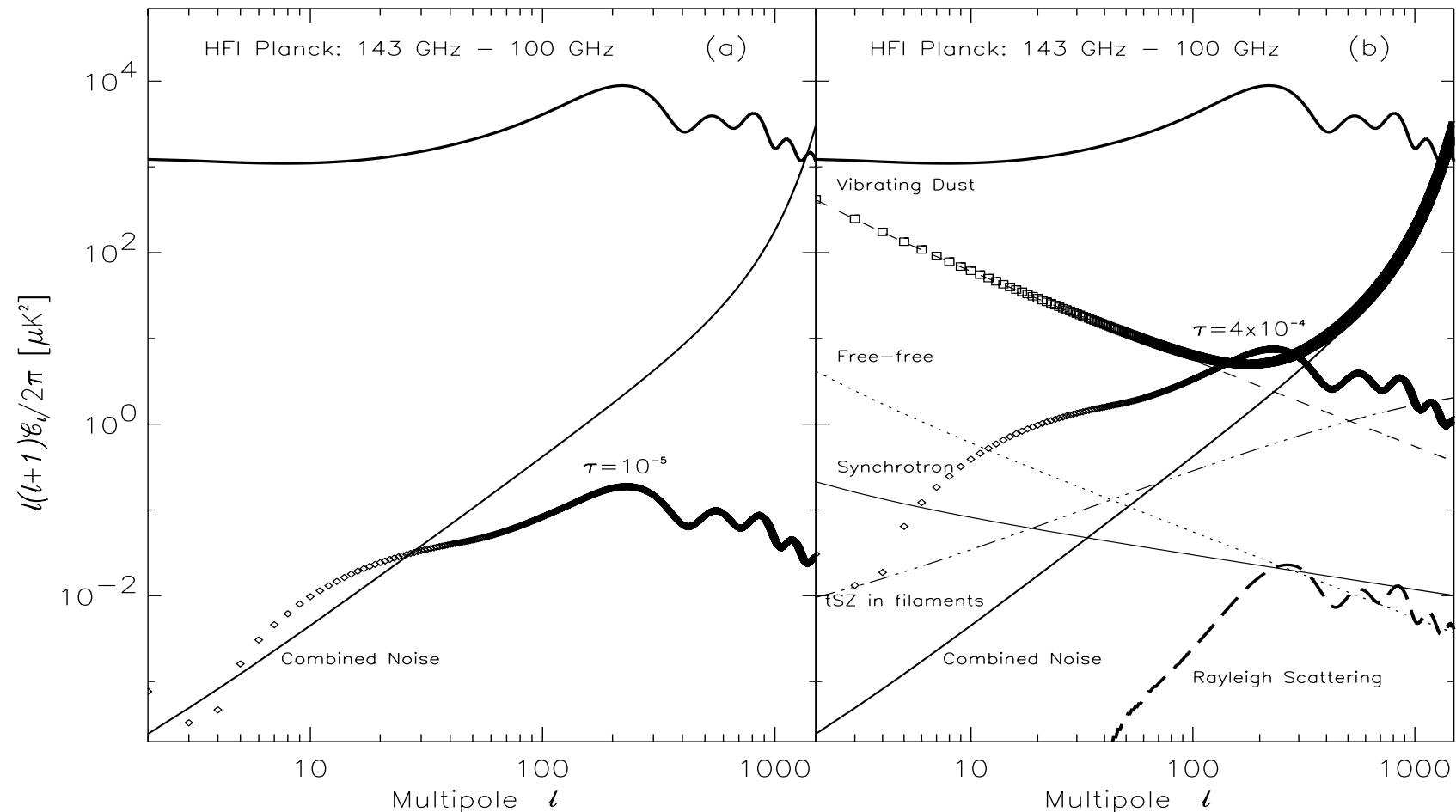


**Fig. 8. a)** Example of optical depth due to a resonant transition which can be detected by the Planck HFI 143 and 100 GHz channels in the absence of foregrounds. The upper thick solid line gives the reference model CMB power spectrum. Diamonds show the expected difference in the power spectrum from both channels due to the resonant scattering placed at  $z = 25$  with  $\tau = 1 \times 10^{-5}$ . **b)** Presence of foreground contamination after subtracting HFI 100 GHz channel from HFI 143 GHz channel. The reference  $\Lambda$ CDM CMB power spectrum is shown in thick solid line, whereas the instrumental noise after the map subtraction is shown in solid intermediate-thickness line. All thin lines refer to the foreground model as quoted as in T00: vibrating dust emission is shown by a dashed line, whereas free-free and synchrotron are given by a dotted and a solid thin line respectively. tSZ effect associated to filaments and superclusters is given by the triple-dot-dashed line. Rotating dust gives negligible contribution at these frequencies. Rayleigh scattering introduces some frequency-dependent variations in the  $C_l$ 's, but well below the noise level (thick dashed line at the bottom right corner). Diamonds show the amplitude of the change in the CMB power spectra induced by resonant species placed at  $z = 25$  and  $\tau = 4 \times 10^{-4}$ .

# Is it going to happen with Planck?

---

- Foreground model is simplistic:
  - We need to know both the spectral dependance and the angular scale dependance extremely well
- Beam uncertainties
- Absolute calibration  $\sim 0.1\%$ , relative better?
- Band-pass uncertainties

# Some questions

---

- Valuable probe of metal enrichment at high redshift. Could we learn anything else?
- Are there any other showstoppers?
- Cross-correlation can certainly help

---

## Carbon monoxide as CMB foreground

Rhigi, Hernandez-Monteagudo, Sunyaev 2008

# CO emission lines

---

- Independent of CMB
- The COs emission lines from early objects at  $0 < z < 10$  is redshifted to 10-115GHz

# CO emission model

- Characterize the galaxies merger distribution using EPS
- Model star forming regions inside this merger using lower z data
- 5% star formation efficiency and starburst lifetime based on simulations
- The star forming regions are quickly enriched by even metals at high redshift
- Assume line luminosity scales as SFR
- Based on high and low z observations

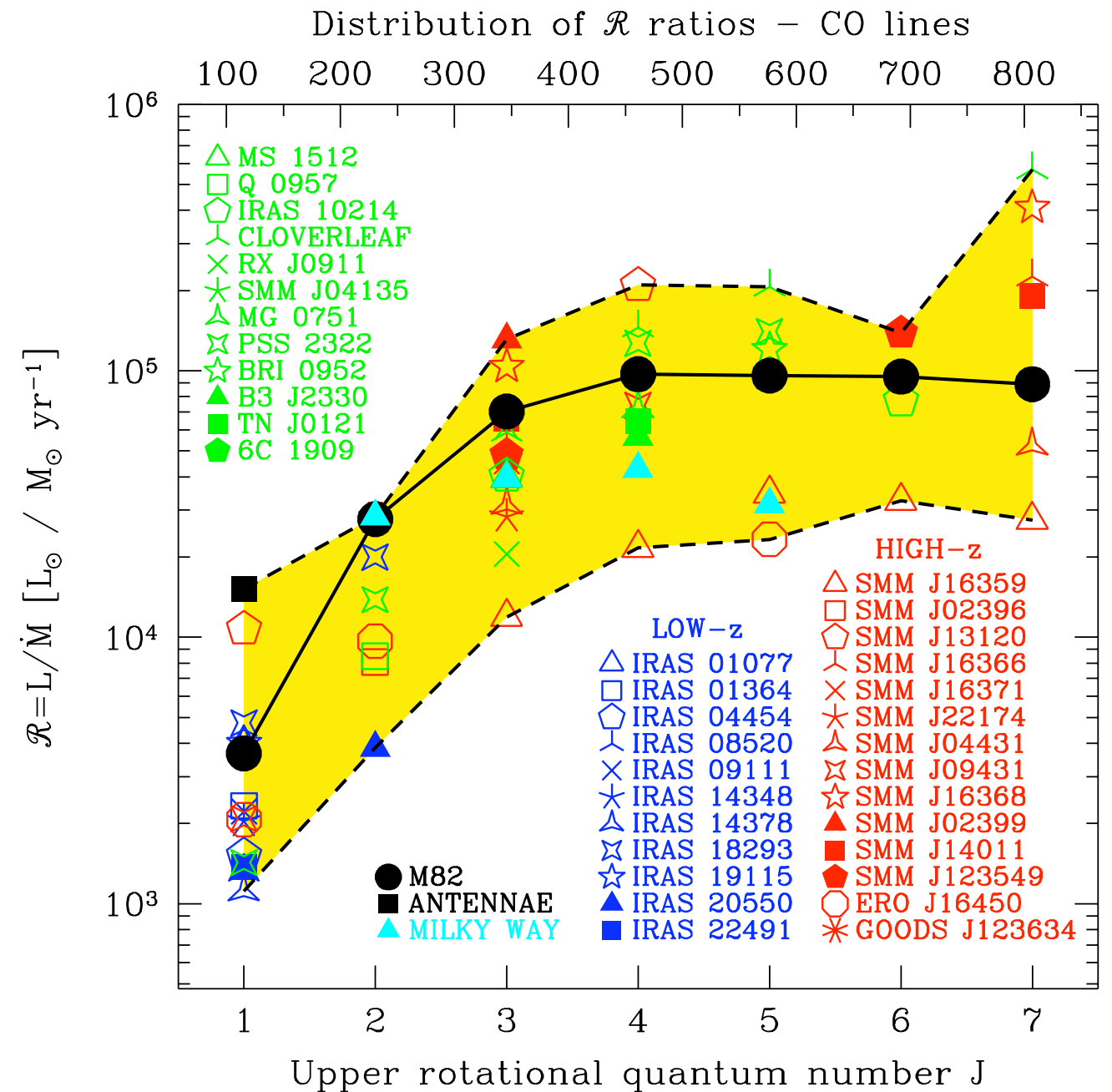


**Fig. 1.** The distribution of the  $\mathcal{R} = L/\dot{M}$  ratios as a function of the upper rotational quantum number of the CO transitions (the corresponding frequency is shown in the upper axis in GHz). Three different samples are considered: low-redshift IRAS galaxies (blue points), high-redshift sub-millimeter galaxies (red points), and high-redshift radiogalaxies and QSOs (Greve et al. 2005; Solomon & Vanden Bout 2005, green points). M82 and the Antennae are shown in black. Our Galaxy (Wright et al. 1991; Cox 2000) is represented with the cyan triangles. See Tables 1 and 2 for details. The black solid line is SED for M82, for which we have data for the full set of lines. Dashed lines represent the upper and lower limits for  $\mathcal{R}$  in the sample.

# Monopole

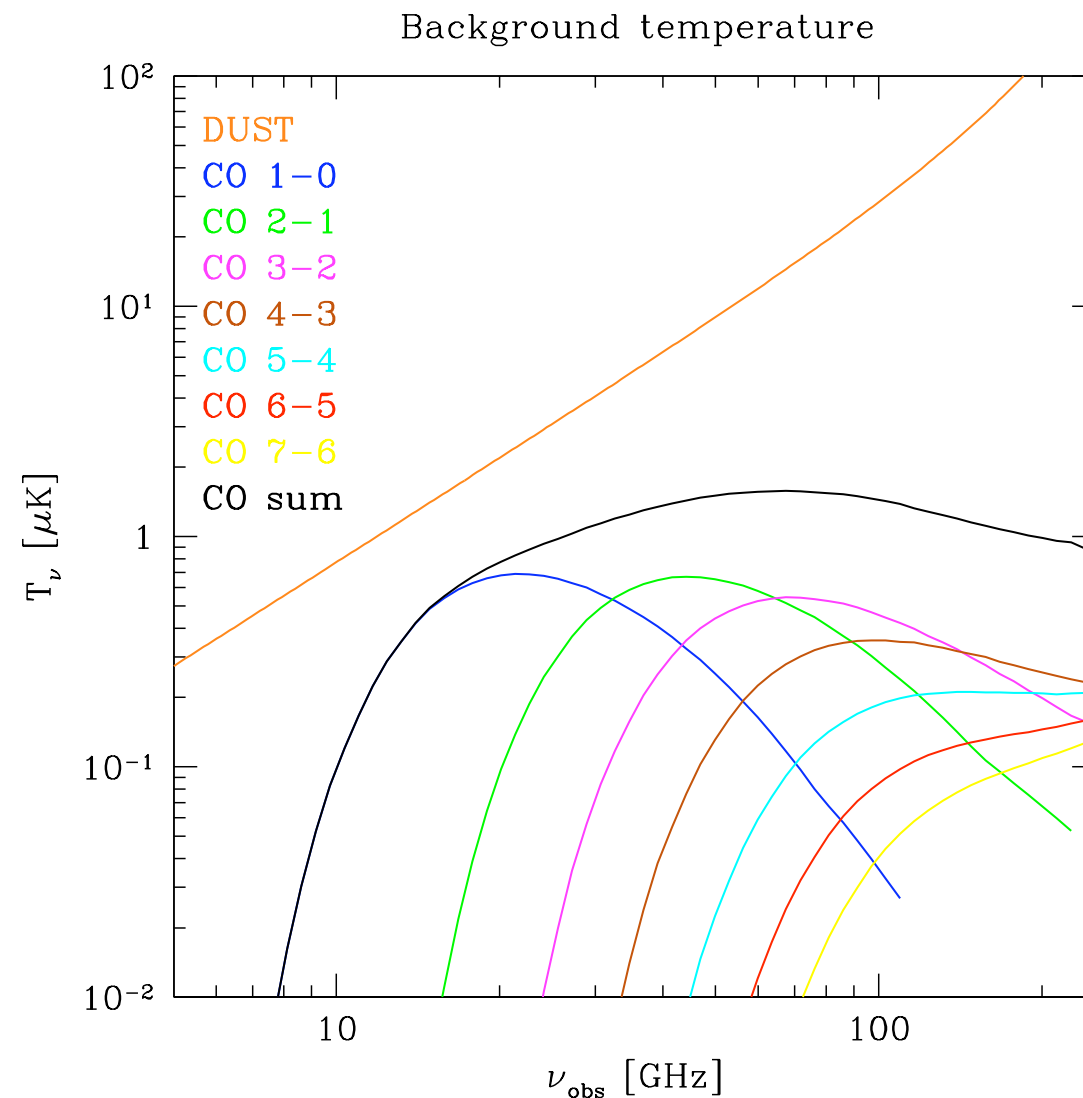


**Fig.4.** The contribution to the cosmic microwave background radiation (in temperature units) from the different CO lines and of their sum (black line), compared with the signal from dust (orange).

- 1000 times weaker than uncertainties in CMB  $T_0$

# Clustering part of the power spectrum

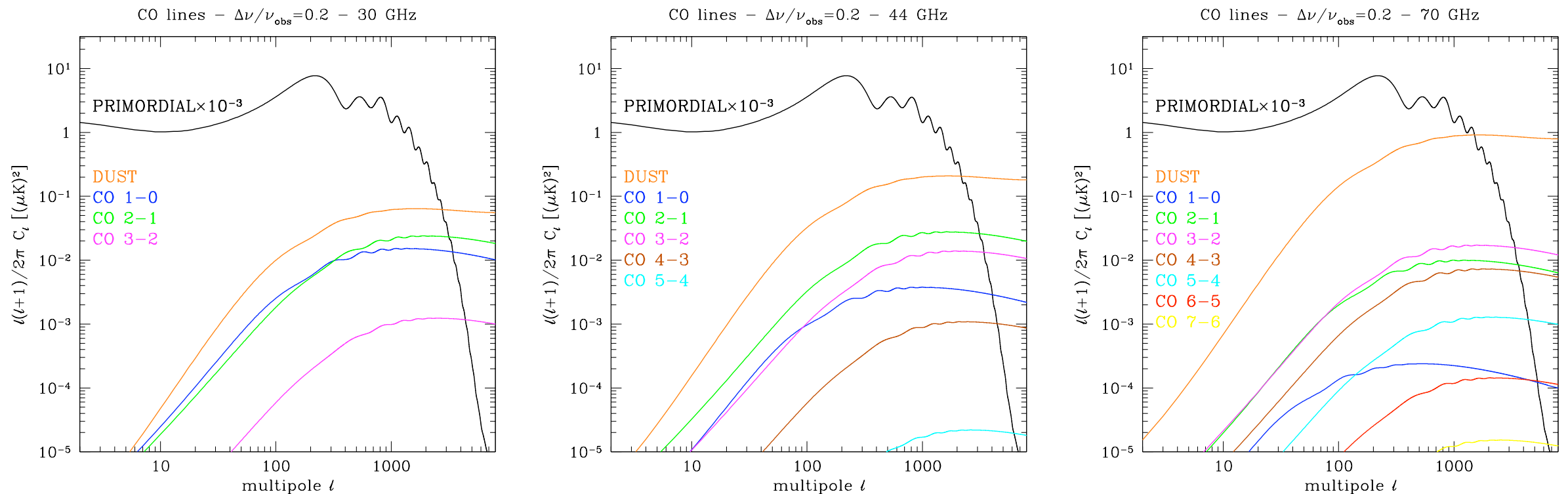


**Fig. 5.** The correlation signal for the CO emission lines at the LFI frequencies and for a spectral resolution  $\Delta\nu/\nu_{\text{obs}} = 0.2$ , using the  $\mathcal{R}$  ratio from M82. The black line is the primordial signal of the CMB divided by 1000, the orange line is the signal from dusty merging star-forming galaxies. Other colors identifies the lines as indicated by the labels.

- Various transitions dominate various frequency range
- Thermodynamic units here
- Emission might be amplified by adjacent CN, HCN, HNC and HCO<sup>+</sup>

# Frequency resolution dependance

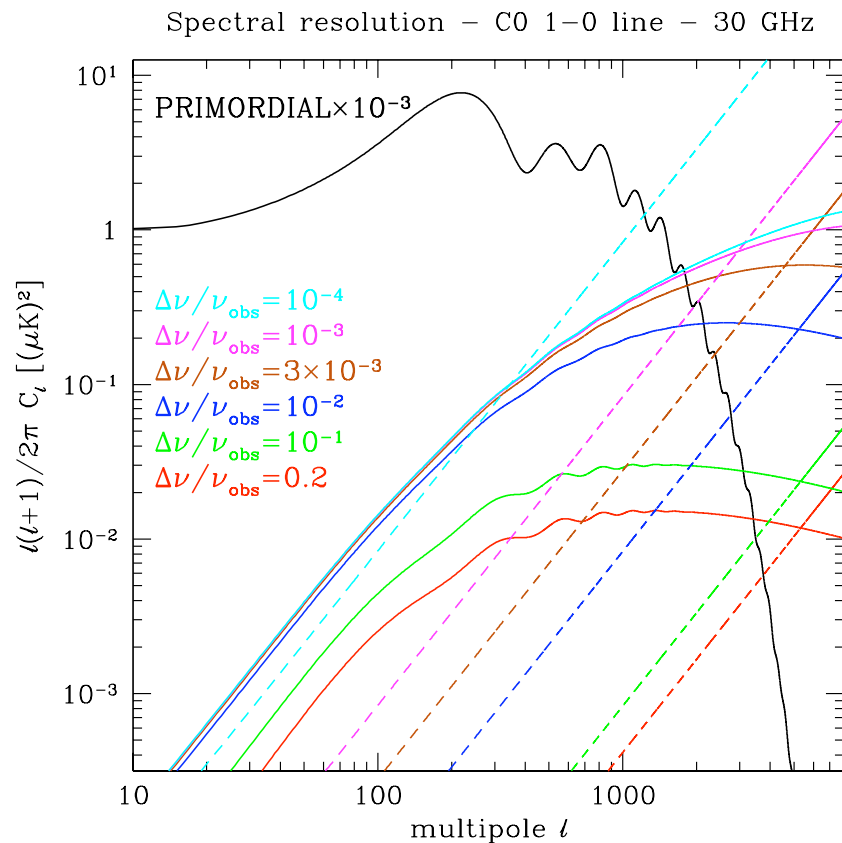


**Fig. 6.** The change in amplitude of the correlation (solid line) and Poisson (dashed line) signal for the CO (1-0) line for different values of the spectral resolution  $\Delta\nu/\nu_{\text{obs}}$ , at 30 GHz. The red and cyan lines are almost superimposed, meaning that, for these resolutions, the signal has already reached a constant value. The Poisson term, on the other hand, grows linearly with decreasing values of the spectral resolution. The primordial signal (black solid line) has been divided by 1000.

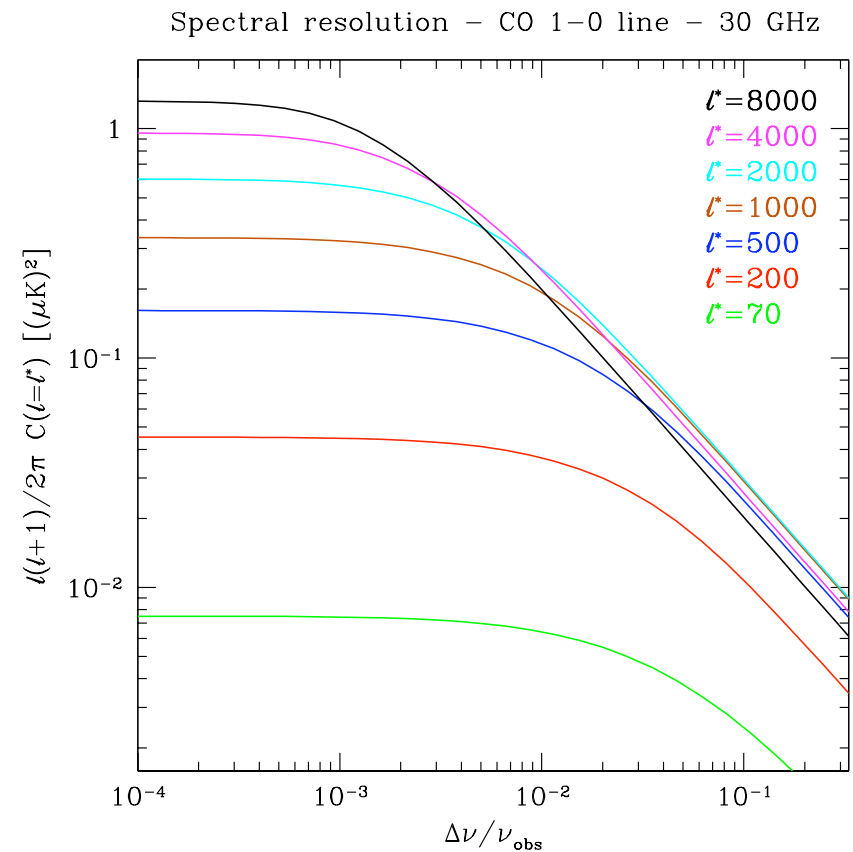


**Fig. 7.** The dependence of the amplitude of the correlation signal on the spectral resolution of the observing instruments, for the CO (1-0) line at 30 GHz and for several value of the multipole index  $l$ .

Given the source number counts, we can compute the contribution of each line to the cosmic microwave background temper-

- Enhancement of the signal when the spectral resolution corresponds to the comoving clustering length
- This introduces a strong spectral resolution dependance

# Optimizing the frequency coverage

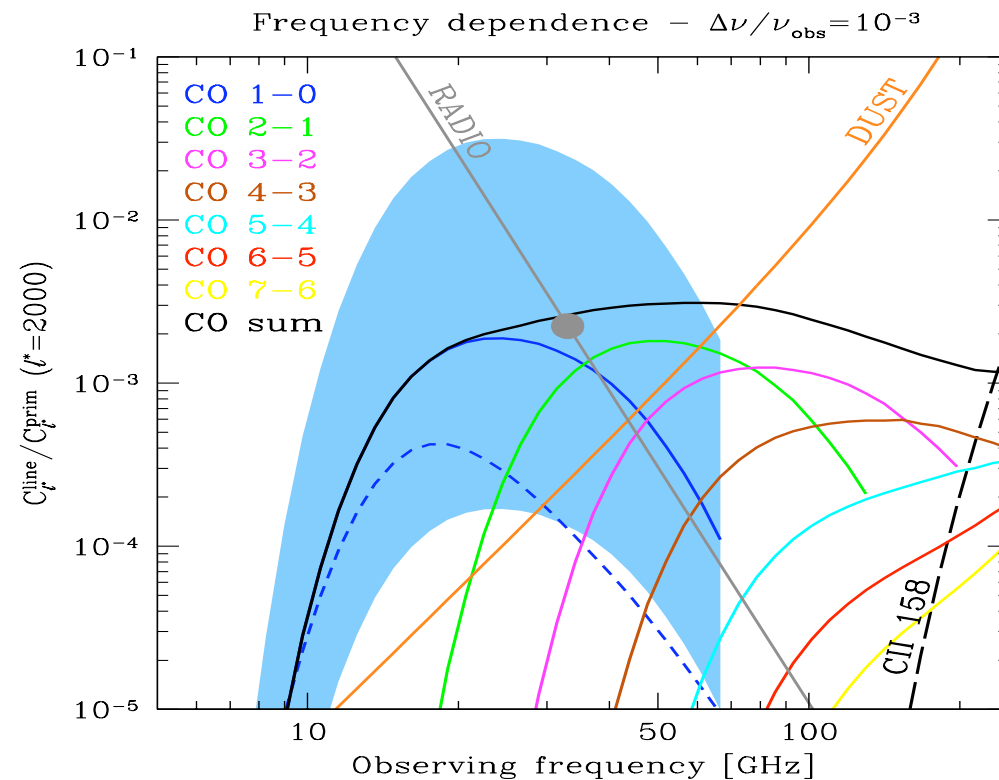


**Fig. 8.** The ratio of the correlation signal from CO emission to the primordial CMB signal at  $l = 2000$  as a function of frequency and for a spectral resolution  $\Delta\nu/\nu_{\text{obs}} = 10^{-3}$ . The black solid line is the sum of the correlation from the first seven CO lines, computed by assuming the  $\mathcal{R}$  ratio for M82. The blue short-dashed line is obtained with the model based on simple Press-Schechter distribution. The black long-dashed line is the signal from CII 158  $\mu\text{m}$  line. The contribution from dust emission in merging galaxies is shown with the orange line. The gray point is the Poisson at 33 GHz from radio sources, estimated from the de Zotti et al. (2005) model, assuming a cutoff of 0.1 mJy. The frequency dependence of this signal (gray line) has been computed assuming  $S_\nu \propto \nu^{-\alpha}$  with  $\alpha = 0.4$  (Toffolatti et al. 2005). The shaded region around the curve for the first CO line represents the range of uncertainties in the correlation signal, according to the different values of  $\mathcal{R}$  for the sample of objects in Fig. 1 and Tables 1 and 2. The first CO line is especially suitable for observations of higher redshifts because, at higher frequencies, we simultaneously observe the contributions from two or three slices of the universe.

# Radio source contribution

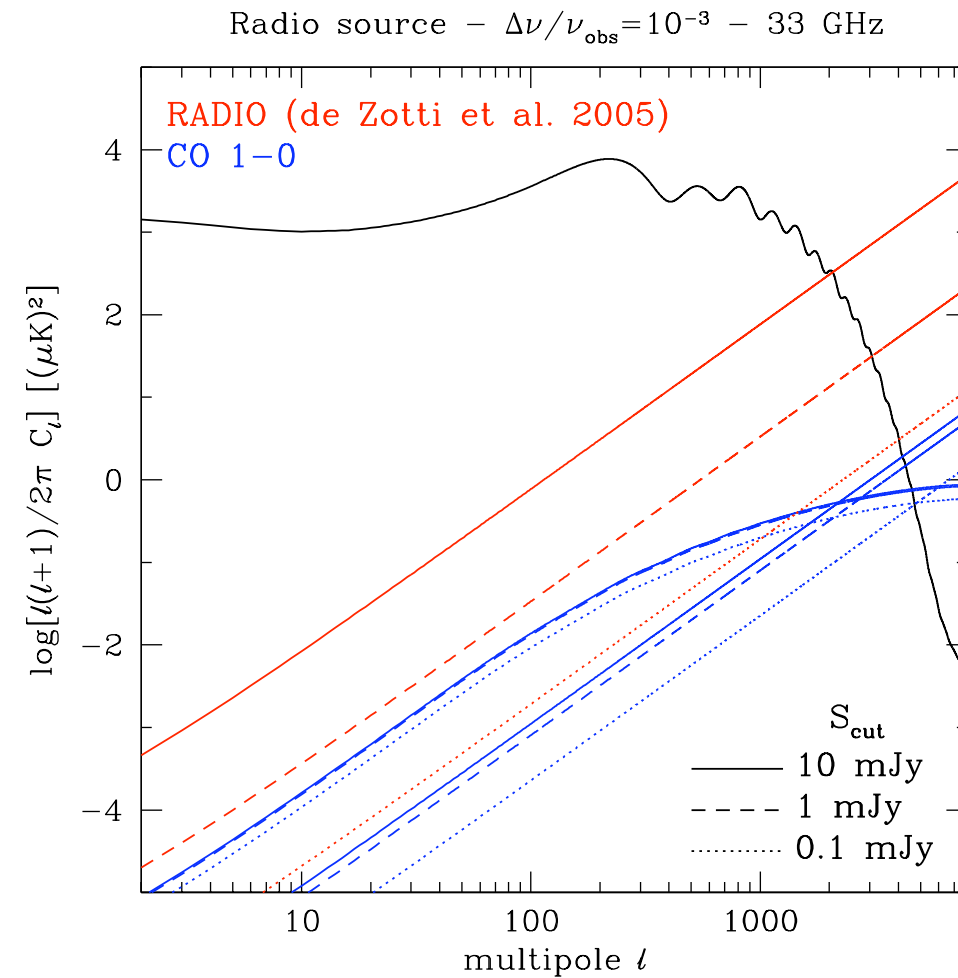


**Fig.9.** The contribution of the radio sources to the power spectrum at 33 GHz (red), compared with the CO (1-0) line (blue). Different flux cutoffs  $S_{\text{cut}}$  are applied: 10 mJy (solid lines), 1 mJy (dashed lines) and 0.1 mJy (dotted lines). The signal due to radio sources is very sensitive to this value, while the power in the CO is much less affected, being generated by sources with fluxes much lower than  $S_{\text{cut}}$ .

# Other atomic lines

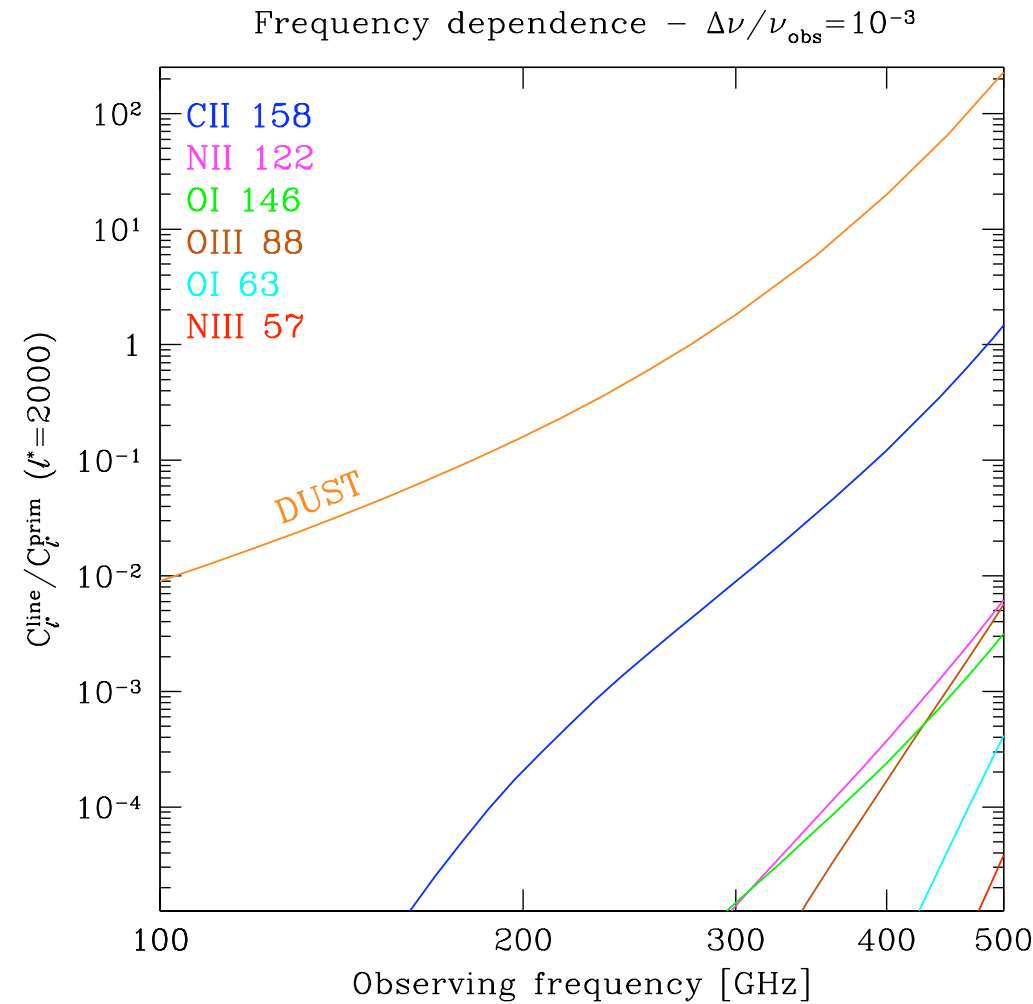


**Fig. 11.** The ratio of the correlation signal from atomic and ionic line emission to the primordial CMB signal at  $l = 2000$  as a function of frequency and for a spectral resolution  $\Delta\nu/\nu_{\text{obs}} = 10^{-3}$ . The orange line is the signal from dust emission in merging galaxies. The CII line clearly dominates the other species, but is below the dust signal even at this spectral resolution.

# Relation to line scattering

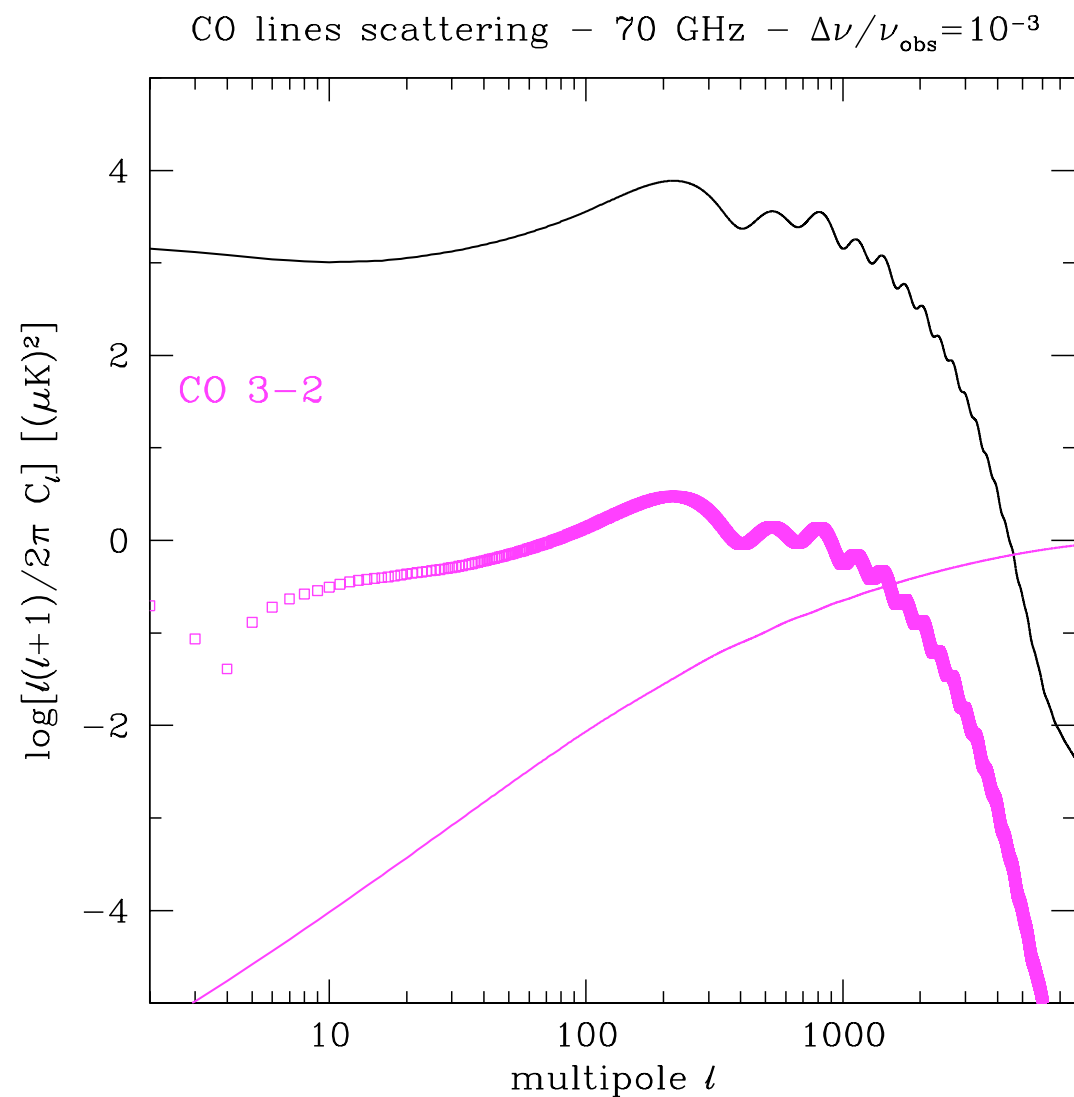


**Fig. 12.** The effect of the scattering of the CO (3-2) line at 70 GHz (squares), according to the model of Basu et al. (2004). The solid line is the correlation term from the emission in the same transition, for a spectral resolution  $\Delta\nu/\nu_{\text{obs}} = 10^{-3}$ .

# Summary and questions

---

- Intermediate windows to probe the same overlapping EOR epoch between low freq. 21cm, and high frequency CII, OI and OIII.
- Star forming regions in the range  $0 < z < 10$ , corresponding to the first CO line to  $\nu \sim 10-115\text{GHz}$
- Should allow different cross-correlation to enhance signal between these various probes.
- Lines cross-correlation calibration can help
- Theoretical uncertainties are probably quite important. We are learning directly about SFR over a wide range of  $z$  (vague statement). Is it better/worse than 21cm?
- Do we learn anything unique?
- Requires both high resolution in spectral ( $\Delta\nu/\nu=10^{-3}$ ) and angular resolution ( $l \sim 2000$ )
- This is 2 orders of magnitude better than Planck/CMBPol (EPIC) and 1 order of magnitude better than CBI. A “super-CBI” seems to be the right experiment
- Foregrounds are still an issue
- Do similar studies for CII exist?
- Does intensity mapping for CO and CII is feasible/make sense?

FIN